

1-28-2007

How Does the Coupling of Secondary and Tertiary Interactions Control the Folding of Helical Macromolecules?

Vikas Varshney

Gustavo A. Carri

University of Akron Main Campus, gac@uakron.edu

Please take a moment to share how this work helps you [through this survey](#). Your feedback will be important as we plan further development of our repository.

Follow this and additional works at: http://ideaexchange.uakron.edu/polymer_ideas

 Part of the [Polymer Science Commons](#)

Recommended Citation

Varshney, Vikas and Carri, Gustavo A., "How Does the Coupling of Secondary and Tertiary Interactions Control the Folding of Helical Macromolecules?" (2007). *College of Polymer Science and Polymer Engineering*. 4.
http://ideaexchange.uakron.edu/polymer_ideas/4

This Article is brought to you for free and open access by IdeaExchange@UAkron, the institutional repository of The University of Akron in Akron, Ohio, USA. It has been accepted for inclusion in College of Polymer Science and Polymer Engineering by an authorized administrator of IdeaExchange@UAkron. For more information, please contact mjon@uakron.edu, uapress@uakron.edu.

How does the coupling of secondary and tertiary interactions control the folding of helical macromolecules?

Vikas Varshney and Gustavo A. Carri^{a)}

Department of Polymer Science, The University of Akron, Akron, Ohio 44325-3909 and The Maurice Morton Institute of Polymer Science, The University of Akron, Akron, Ohio 44325-3909

(Received 1 June 2006; accepted 5 December 2006; published online 29 January 2007)

The authors study how the simultaneous presence of *short-range* secondary and *long-range* tertiary interactions controls the folding and collapse behavior of a helical macromolecule. The secondary interactions stabilize the helical conformation of the chain, while the tertiary interactions govern its overall three-dimensional shape. The authors have carried out Monte Carlo simulations to study the effect of chain length on the folding and collapse behavior of the chain. They have calculated state diagrams for four chain lengths and found that the physics is very rich with a plethora of stable conformational states. In addition to the helix-coil and coil-globule transitions, their model describes the coupling between them which takes place at low temperatures. Under these conditions, their model predicts a cascade of continuous, conformational transitions between states with an increase in the strength of the tertiary interactions. During each transition the chain shrinks, i.e., collapses, in a rapid and specific manner. In addition, the number of the transitions increases with increasing chain length. They have also found that the low-temperature regions of the state diagram between the transition lines cannot be associated with specific structures of the chain, but rather, with ensembles of various configurations of the chain with similar characteristics. Based on these results the authors propose a mechanism for the folding and collapse of helical macromolecules which is further supported by the analysis of configurational, configurational, and thermodynamic properties of the chain. © 2007 American Institute of Physics. [DOI: 10.1063/1.2428298]

I. INTRODUCTION

Understanding the molecular mechanisms that lead to the folding or collapse of macromolecules as a consequence of changes in environmental conditions such as a decrease in temperature, solvent quality, and other physical variables is a first-class challenge in polymer physics.¹ Perhaps, the most illustrative example of this problem can be found in the coil-globule transition, i.e., the collapse transition, typically observed in synthetic polymers as well as biopolymers. Due to the relevance of this transition to various macromolecular systems such as polymer solutions, network collapse, protein folding, DNA packaging, and others, extensive experimental²⁻⁸ theoretical,⁹⁻¹¹ as well as computer simulation¹²⁻¹⁶ studies have been carried out to fully understand this transition. While a significant amount of information about the conformation and configuration of the chains has been gained through experimental techniques such as scanning force microscopy,⁴ dynamic light scattering,⁵ fluorescence measurements,⁶ and others; theoretical and computer simulation studies have complemented the experimental observations and led to a deeper understanding of the thermodynamics of the coil-globule transition.

It is well known that some macromolecules can also adopt equilibrium conformations other than the random coil and globular state. One of such conformations is the helical conformation which is commonly observed in synthetic as

well as biological polymers. If helical and globular conformations can form simultaneously, then a coupling and competition between the helix-coil and coil-globule transitions can be expected which may result in a novel and rich physical behavior of the macromolecule. Biopolymers such as proteins and DNAs belong to this category and put forward a more realistic picture of such conformational changes present in macromolecules. Interestingly, the possibility of this coupled behavior between the coil-globule and helix-coil transitions has been explored theoretically by Saven and Wolynes,¹⁷ and via computer simulations by Chou and Shakhnovich to some extent.¹⁸ It has also been suggested by Di Marzio¹⁹ as one particular case of a more general classification of possible couplings of phase transitions in macromolecular systems. Recently, Matsuyama²⁰ has studied one such coupling between the behavior of a polymer threading a membrane and the coil-globule transition.

The helix-coil transition is one of many important conformational changes occurring in biopolymers and has been extensively reviewed by Poland and Scheraga.²¹ Indeed, the helix-coil transition is the consequence of a competition between the enthalpically favored, intramolecular, short-range (*along the contour of the polymer chain*) hydrogen bonds between nearby residues and the overall entropy of the chain. In addition, long-range interactions (*along the contour of the polymer chain*) such as electrostatic interactions, van der Waals interactions, and long-range hydrogen bonds also do play a very significant role in determining the overall shape of the macromolecule. At this point, let us digress briefly and

^{a)}Author to whom correspondence should be addressed. Electronic mail: gac@uakron.edu

clarify the terminology that we will employ in the rest of this paper. We define short-range interactions as those interactions involving residues that are close to each other *along the contour of the polymer chain*. Long-range interactions are those involving residues that are *far apart along the contour of the polymer chain* even though they might be spatially close to each other. Therefore, interactions such as van der Waals interactions that die off very quickly as a function of distance are treated as long-range interactions in the present manuscript.

Interestingly, in proteins,²² it is the delicate balance between aforementioned short- and long-range interactions which determines its three-dimensional conformational state. Thus, helical macromolecules provide us with an excellent opportunity to explore the conformational space of macromolecules where both short- and long-range interactions are relevant. These systems will display the coupling between the helix-coil and coil-globule transitions where short-range interactions stabilize the helical state while long-range interactions control the overall three-dimensional shape and entropy favors the random-coil state.

Due to the hierarchical structure of proteins, it is quite a challenge at present to explore the above transitions and their possible coupling using deterministic approaches such as molecular dynamics simulations due to computational limitations. However, with the advent of algorithms capable of escaping energy minima, such as the multicanonical²³ and Wang-Landau algorithms,²⁴ it is possible to address the coupling of transition in macromolecular systems using stochastic approaches such as Monte Carlo simulations. In particular, the Wang-Landau algorithm and various modifications of it have been extensively used to address studies on lattice models,²⁵ united atom models for proteins,²⁶ ring polymers,²⁷ HP model,²⁸ RAFT model,²⁹ pair potentials for proteins,³⁰ sequence based and structure based energy functions for proteins,³¹ the collapse of semiflexible¹⁵ and flexible¹⁶ polymers, etc. Recently, we have proposed a minimal model³² to model the helix-coil transition in homopolypeptides using Monte Carlo simulations based on the Wang-Landau sampling algorithm. Furthermore, we extended our study further to understand the aforementioned coupling behavior.³³ Our model is a minimal model tailored to study helical conformations *only*. Thus, potentials for the formation of other secondary structures such as beta hairpins and sheets were not included.

Our previous simulations were motivated to understand the coupling behavior between the helix-coil and coil-globule transitions for homopolypeptides. A rich state diagram was obtained for a chain of 60 beads. In the present article, we extend the study to explore the changes in the state diagram and other physical properties induced by changes in the length of the chain. Specifically, we study chains of 10, 30, 45, and 60 beads, and analyze the behaviors of various conformational, configurational, and thermodynamic properties.

The rationale for the study of the effect of chain length is that this molecular parameter is one of the most important ones in polymeric systems. The physical characteristics of

various transitions such as the helix-coil transition depend on the length of the chain.²¹ Furthermore, in the limit of infinite molecular weight, some transitions become *true thermodynamic transitions*³⁴ and even the physical nature of the transition might be changed.³⁵ Another motivation for this study is that chain length might modify the effective strengths of short- and long-range interactions differently; thus, shifting the state diagram. Indeed, this turns out to be the case for our model.

This article is organized as follows. In the next section, we describe our simulation protocol where we present a brief description of the model followed by our simulation methodology. In the following section, we present our simulation results along with their discussion. First, we present the state diagrams for all the chain lengths studied which are discussed and compared in terms of possible stable states in the various regimes. Then, in order to enhance our understanding of the various regimes in the state diagrams, we discuss our results in terms of conformational, configurational, and thermodynamic properties. Finally, we conclude the article by summarizing the most important findings of our work and with appropriate acknowledgments.

II. MODEL AND SIMULATION PROTOCOL

A. The model

The various aspects of our minimal model have already been published in detail elsewhere.³² Here we present a brief, conceptual description and extend it further to study the effect of long-range, interbead interactions on the helix-coil transition of the chain and its equilibrium properties. In our minimal model a polypeptide molecule is mapped onto the freely rotating chain model³⁶ where each amino acid residue is represented by a bead. The well known cooperative nature³² of this transition has been captured using a geometrical criterion based on the concept of “torsion” of a curve which is a well defined mathematical quantity.³⁷ More precisely, in our model the cooperativity arises from the entropic penalties related to the nucleation and propagation of helical sequences. While the nucleation of a helical sequence restricts two consecutive dihedral angles; thus, restricting the torsion of two consecutive beads and the spatial positions of five consecutive beads, the propagation restricts only one dihedral angle, i.e., it restricts the torsion of only one bead and the spatial positions of four consecutive beads. The use of torsion to mimic hydrogen bonding in homopolypeptides along with the freely rotating chain model has been discussed in detail previously.³² We have employed the concept of torsion as a criterion to determine the conformational state (helix or coil) of each bead. A helical bead carries a negative enthalpy, called C , which stabilizes the helical conformation; otherwise, the bead is in the random-coil state which is taken as the reference state of the system. The enthalpic parameter C is related to the standard parameter s of helix-coil transition theory²¹ as follows:

$$s = \exp(-\Delta F/k_B t) \quad \text{where } \Delta F = C - T\Delta S. \quad (1)$$

The enthalpic parameter C was kept constant in the simulations and tuned such that the helix-coil transition occurs

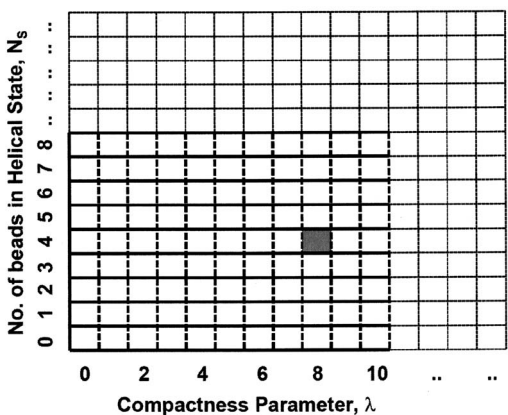


FIG. 1. Schematic of the distribution of bins with respect to the beads in the helical state, N_s , and the compactness parameter, λ .

around $T_{hc} \sim 300$ K. This parameter provides the enthalpic contribution that arises from the formation of a hydrogen bond. Furthermore, ΔS is the decrease in the entropy of the residue incorporated into a helical sequence due to the formation of a new hydrogen bond. The origin of ΔS in our model arises from the freely rotating chain model and the constraints in the dihedral angles. Both parameters C and ΔS are negative in Eq. (1).

At this point it is important to mention two important limitations of our model. First, in real systems residues far away from each other (along the contour of the chain) might be spatially close enough to form hydrogen bonds; this might lead to other secondary structures such as beta hairpins.³⁸ We did not consider this possibility when building our model; we wanted to develop a minimal model for the formation of helices. The formation of such *long-range* hydrogen bonds would need a different potential energy and add to the complexity of the problem. Second, the purpose of our model is

to study the generic features of the coupling between the helix-coil and coil-globule transitions. Any property that is a direct consequence of the *specific* chemistry of the chain should not be addressed with our model. For example, our model cannot address the nucleation of helices that start in *specific* residues on the chain.

B. Modeling nonlocal interactions

In the present simulations, the effects of long-range, interbead interactions are modeled with a modified Lennard-Jones potential of the form

$$V_{ij} = 4\epsilon \left(\left(\frac{\sigma}{r_{ij}} \right)^{12} - \left(\frac{\sigma}{r_{ij}} \right)^6 \right), \quad r_{ij} \geq \sigma, \quad (2a)$$

$$V_{ij} = \infty, \quad r_{ij} < \sigma, \quad (2b)$$

where r_{ij} is the distance between beads i and j , ϵ is the strength of the interaction, and σ the bead diameter. The potential is summed over all pairs (1-2 and 1-3 interactions are *not* included) to obtain the total interaction energy for a particular configuration of the chain. As shown in Eq. (2b), the excluded volume interactions were modeled using hard core potential energies, i.e., all the configurations with any r_{ij} less than σ were discarded. Hence, only negative contributions were considered when calculating the total long-range interaction energy.

We note that the quantity $\sum_i \sum_{j>i} V_{ij}/\epsilon$ depends only on the configuration of the chain and is independent of ϵ . Thus, we define the compactness parameter λ as follows: $\lambda = -\sum_i \sum_{j>i} V_{ij}/\epsilon$, which is proportional to the long-range interaction energy of the system. By definition large values of λ correspond to more compact configurations; consequently, λ is capable of detecting globular conformations of the chain.

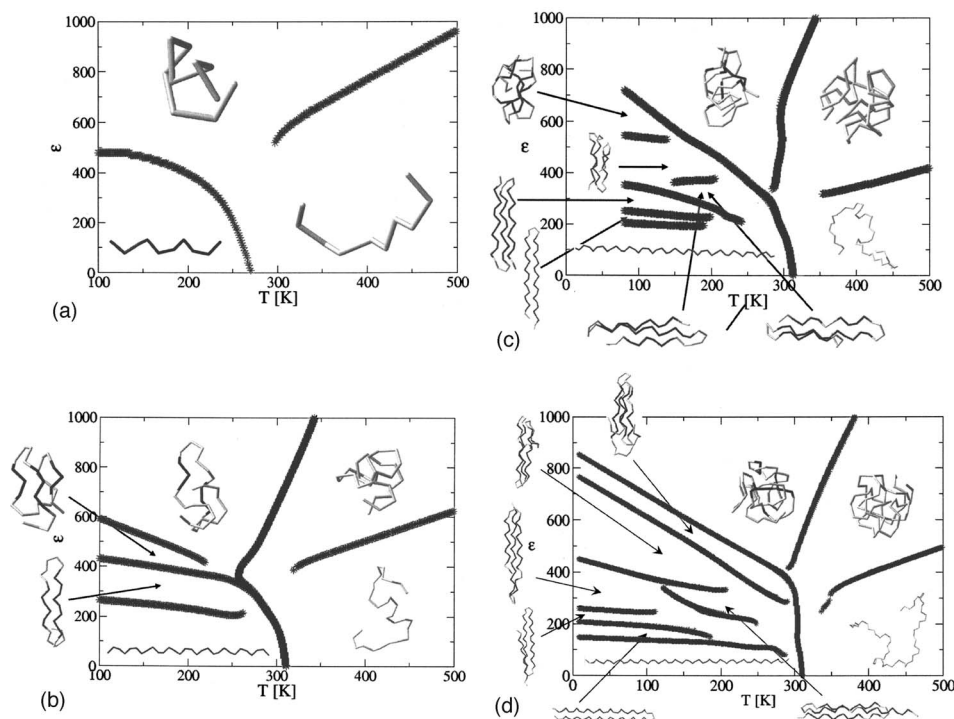


FIG. 2. (a) State diagram for a chain with 10 beads. Helical beads (dark segments); coil beads (light segments). (b) State diagram for a chain with 30 beads. Helical beads (dark segments); coil beads (light segments). (c) State diagram for a chain with 45 beads. Helical beads (dark segments); coil beads (light segments). (d) State diagram for a chain with 60 beads. Helical beads (dark segments); coil beads (light segments).

C. Simulation methodology

Let us consider an arbitrary configuration of the polymer chain which is generated during the course of the simulation. This configuration contains two relevant parameters of interest: the number of beads in the helical state, N_s , and the compactness parameter, λ , that quantifies the global packing of the chain. The former is a measure of local interactions, while the latter is a consequence of the nonlocal, tertiary interactions. Then, we write the energy for this configuration as follows:

$$E = CN_s - \varepsilon\lambda. \quad (3)$$

It is clear from Eq. (3) that the energy of a configuration depends on N_s and λ , and can be written as $E = E(N_s, \lambda)$. C and ε are the energy parameters for hydrogen bonds and van der Waals interactions, respectively.

Each energy state is associated with a number of possible configurational states; thus, the total number of configurational states per unit energy is defined as the density of states (DOS), $g(E)$. Therefore, $g(E)$ can be written as a function of N_s and λ . We denote it as $g(N_s, \lambda)$. This dependence of the DOS on N_s and λ is illustrated in Fig. 1. In this schematic, which consists of many small squares, the vertical axis corresponds to the number of beads in the helical state, N_s , which increases stepwise, while the horizontal axis corresponds to the total attractive interaction for each configuration as quantified by λ , which is a continuous variable. We discretize this horizontal axis by binning it in intervals of width equal to α . The values of α were taken as 1, 1, 4, and 5 for chain lengths of 10, 30, 45, and 60, respectively. Therefore, any configuration generated by the simulation can be assigned to one of the squares shown in Fig. 1. For example, if the configuration of the chain with length equal to 45 beads has four helical beads and $\lambda = 33.57$, then this configuration would be assigned to the shaded bin in Fig. 1.

We estimate the density of states for our model using Monte Carlo simulations based on the two-dimensional version of the Wang-Landau sampling algorithm²⁴ as first implemented by Yan *et al.*³⁹ The details of our simulation procedure have been described previously in the case of the force-elongation relationship of homopolypeptides.⁴⁰ Here, we would also like to mention that for chain lengths equal to 45 and 60 beads, the simulation was performed using the distributed implementation of the Wang-Landau algorithm suggested by Schulz *et al.*⁴¹ which is described below.

The bin diagram shown in Fig. 1 was divided into 8 and 24 horizontal windows for chain lengths of 45 and 60, respectively; in such a way that each window covered a small range of values for the number of helical beads, N_s , and the whole range of possible values of the compactness parameter, λ . Moreover, the boundaries of consecutive windows were chosen such that they overlapped. Afterward, each window was simulated using the Wang-Landau algorithm *independently*, as suggested by Schulz *et al.*,⁴¹ considering boundary effects to estimate DOS. When the DOS for each window was known, the overlapping portions of consecutive windows were used for the overall matchup and rescaling of

the global density of states for the whole range of N_s and compactness parameter λ .

Once the DOSs were known, they were further rescaled to get true density of states, $g_{\text{true}}(N_s, \lambda)$, as follows:

$$g_{\text{true}}(N_s, \lambda) = \frac{g(N_s, \lambda)}{\sum_{N_s, \lambda} g(N_s, \lambda)} X \text{Tot}_{\text{conf}}, \quad (4)$$

where Tot_{conf} is the total number of possible configurations that the chain could take which, for our model, is 64^{N-3} , N being the number of beads in the chain. Once $g_{\text{true}}(N_s, \lambda)$ is known, various ensemble averages of interest can be calculated using standard formulas of statistical mechanics. For example, the mathematical expressions for the canonical partition function, Helmholtz free energy, internal energy, entropy, and heat capacity are

$$Z(T, \varepsilon) = \sum_{N_s, \lambda} g_{\text{true}}(N_s, \lambda) e^{-\beta(CN_s - \varepsilon\lambda)}, \quad (5)$$

$$A(T, \varepsilon) = -T \ln \left(\sum_{N_s, \lambda} g_{\text{true}}(N_s, \lambda) e^{-\beta(CN_s - \varepsilon\lambda)} \right), \quad (6)$$

$$U(T, \varepsilon) = \langle E \rangle_T = \frac{\sum_{N_s, \lambda} g_{\text{true}}(N_s, \lambda) (CN_s - \varepsilon\lambda) e^{-\beta(CN_s - \varepsilon\lambda)}}{\sum_{N_s, \lambda} g_{\text{true}}(N_s, \lambda) e^{-\beta(CN_s - \varepsilon\lambda)}}, \quad (7)$$

$$S(T, \varepsilon) = \frac{U(T, \varepsilon) - A(T, \varepsilon)}{T}, \quad (8)$$

$$C_V(T, \varepsilon) = \frac{\langle E^2 \rangle_T - \langle E \rangle_T^2}{T^2}, \quad (9)$$

where $A(T, \varepsilon)$, $U(T, \varepsilon)$, $S(T, \varepsilon)$, and $C_V(T, \varepsilon)$ are in units of Boltzmann's constant, k_B , and β is the reciprocal absolute temperature, i.e., T^{-1} . Apart from these thermodynamic quantities, the ensemble average of any other quantity of interest, $\langle AA \rangle$, can also be calculated as follows:

$$\langle AA(T, \varepsilon) \rangle = \frac{\sum_{N_s, \lambda} g_{\text{true}}(N_s, \lambda) (AA(N_s, \lambda)) e^{-\beta(CN_s - \varepsilon\lambda)}}{\sum_{N_s, \lambda} g_{\text{true}}(N_s, \lambda) \cdot e^{-\beta(CN_s - \varepsilon\lambda)}}. \quad (10)$$

III. RESULTS AND DISCUSSION

A. State diagrams

We start our discussion with a brief description of the state diagrams. Figures 2(a)–2(d) show the state diagrams for chain lengths equal to 10, 30, 45, and 60 beads, respectively. All figures show the existence of stable configurational states of the polymer chain in various regions of the state diagrams. In all cases, the dark and light segments represent helical and coil beads, respectively. The boundaries shown in the state diagrams describe the transitions from one configurational state to another one and were obtained from the peak in the heat capacity, C_v (as function of ε and T). The figures also show many boundaries (small peaks in C_v) ending before merging with the other boundaries (large peaks). This occurs

when the smaller peak approaches the large one; it becomes shoulder or is completely absorbed by the large peak; hence, such peaks could not be resolved numerically. Interestingly, all the state diagrams depict similar configurations of the chain in the limiting regimes; i.e., a helical configuration for small values of ε and at low T , a random-coil configuration for small values of ε and at high T , an amorphous globular configuration for large values of ε and at high T , and a globular configuration with residual secondary structure for large values of ε and at low T which results from the competition between long-range attractive interactions among the beads and the favored secondary structure due to stabilization of helical beads. The latter configuration is not observed in Fig. 2(a) due to the short length of the polymer.

The aforementioned configurations at low T and high ε mimic the globular configurations of some proteins where residual secondary structure persists even in globular state.⁴² In such cases [Figs. 2(b)–2(d)], we also observe the emergence of a few more regimes in the low-temperature limit as ε increases. These regions of the state diagram do not correspond to one specific structure of the polymer chain but rather to an ensemble of configurations with similar characteristics. Snapshots of the polymer taken from the simulations are shown in the figures.

Let us now consider each region separately. Firstly, in the low ε limit and at low temperatures, the chain is stable in the helical configuration which, upon an increase in temperature, undergoes the traditional helix-coil transition.³² Secondly, in high T limit, the chain undergoes the standard coil-globule transition with an increase in ε . Thirdly, in low T limit, we observe a cascade of *continuous conformational* transitions starting from a perfect helical state for small values of ε and ending in a collapsed globular state with residual secondary structure; except in the case of very short chains, Fig. 2(a). However, when comparing the various state diagrams, we found that the number of these low-temperature transitions increases with increasing chain length. For example, we find that for 30, 45, and 60 beads, we have 3, 5, and 6 continuous transitions, respectively. These transitions give rise to various configurations that are present in all the state diagrams [Figs. 2(b)–2(d)]. The emergence of these transitions is a consequence of the competition between interbead attractive interactions, which bring the beads closer to each other, and the torsional energy which stabilizes the helical configuration of the chain. This competition results in the breaking of the helical structure with increasing ε such that, once the structure is broken, it adopts a configuration that minimizes the Lennard-Jones (LJ) interaction energy. This is achieved by folding the helical strands into a parallel arrangement such that they are close to each other. For example, during the first transition a perfect helical structure gets transformed into a hairpinlike structure in all the state diagrams. Further analysis of all the regimes and various transitions is done in the remaining subsections using various configurational, conformational, and thermodynamic properties of the chain.

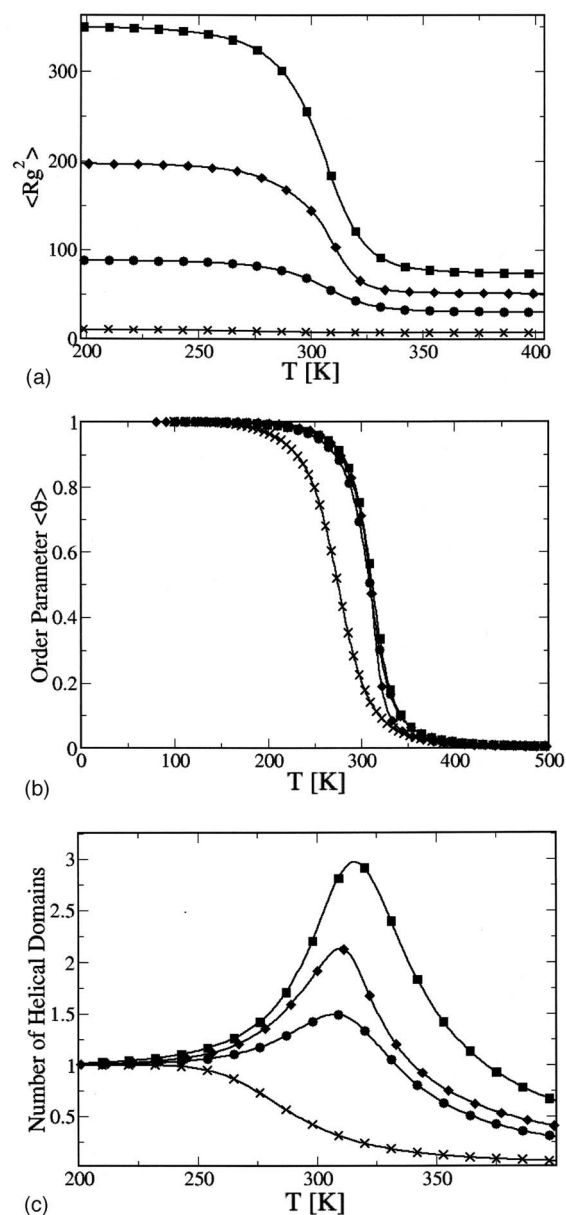


FIG. 3. (a) Plot of the mean square radius of gyration, $\langle R_g^2 \rangle$, as a function of temperature, T , for various chain lengths. The parameters are (*) $N=10$ beads, (●) $N=30$ beads, (◆) $N=45$ beads, and (■) $N=60$ beads. (b) Plot of the order parameter, $\langle \theta \rangle$, as a function of temperature, T , for various chain lengths. The parameters are (*) $N=10$ beads, (●) $N=30$ beads, (◆) $N=45$ beads, and (■) $N=60$ beads. (c) Plot of the number of helical domains, $\langle N_H \rangle$, as a function of temperature, T , for various chain lengths. The parameters are (*) $N=10$ beads, (●) $N=30$ beads, (◆) $N=45$ beads, and (■) $N=60$ beads.

B. Effect of chain length on configurational, conformational, and thermodynamic properties

1. The low ε regime

All the state diagrams show the presence of the standard helix-coil transition for small values of ε . Since we have discussed this transition in detail recently,³² we only present a brief description of the chain length dependence of the various properties. The mean square radius of gyration, $\langle R_g^2 \rangle$, is plotted as a function of T in Fig. 3(a) for four chain lengths. It is clear from the figure that for all cases, $\langle R_g^2 \rangle$ decreases with increasing temperature indicating the pres-

ence of a transition where the chain changes its configuration from an extended one to a more compact one. In addition, Fig. 3(b) illustrates the cooperative nature of this transition through the typical sigmoidlike shape of the order parameter $\langle \theta \rangle$ (i.e., helical content) as a function of T . The transition occurs at T_{hc} which is determined by the parameter C of our model. At low temperatures, the helical content is one implying an all-helical configuration but, as the temperature increases, the helical content decreases to zero indicating the melting of the helical strands. Further insight regarding the breaking mechanism of the helical structure with increasing temperature can be obtained from Fig. 3(c) where the number of helical domains, $\langle N_H \rangle$, is plotted as a function of T . The peak around T_{hc} indicates that the helical structure breaks into more than one helical strand during the transition, in agreement with helix-coil transition theories.²¹ Moreover, $\langle N_H \rangle$ increases with increasing chain length indicating that the longer the chain, the larger the number of intermediate helical strands during the transition. However, for short chains $\langle N_H \rangle$ decreases monotonically which indicates that the chain unwinds from the ends during the transition.

2. The high T regime

As mentioned previously, the coil-globule transition is observed in the high-temperature regime as a function of ϵ . In this temperature regime the helical conformation is unstable; thus, it is absent and no interference with the coil-globule transition occurs. Therefore, at low values of ϵ , the chain adopts the random-coil configuration due to the dominance of entropy. However, as the magnitude of ϵ is increased, the chain starts to collapse leading to the coil-globule transition. This is confirmed by Fig. 4(a) where the normalized chain dimension, as quantified by mean square radius of gyration divided by N , $\langle R_g^2 \rangle / N$, is plotted as a function of ϵ for chain lengths of 30, 45, and 60 beads, respectively. Firstly, the figure clearly shows the decrease in chain dimensions indicating the collapse of the polymer chain which reaches a plateau for large values of ϵ . Secondly, we observe a change in the trend of $\langle R_g^2 \rangle / N$ for various chain lengths. Interestingly, the crossover of this feature occurs around $\epsilon \sim 200$ where the normalized chain dimensions are the same for all the chain lengths studied. This suggests that the attractive interactions at $\epsilon \sim 200$ are enough to overcome the effect of excluded volume interactions due to hard core repulsions. For values of ϵ below 200, the excluded volume interactions control the behavior of the chain while, for values of ϵ above 200, the attractive interactions are dominant and lead to the collapse of the chain.

We have observed that the scaling law $\langle R_g^2 \rangle / N \propto N^\alpha$ is valid over the entire range of values of ϵ . The exponent α was found to be positive for small values of ϵ , approximately zero for $\epsilon \sim 200$, and negative for values of ϵ above 200. Specifically, we found the values of α to be 0.28, -0.01 , and -0.21 for $\epsilon = 0, 200$, and 800 . From Fig. 4(a), it is also clear that the transition becomes sharper with increasing chain length. Moreover, it also shows that the collapse of the chain shifts towards lower values of ϵ as the chain length increases. This is the direct consequence of the interbead at-

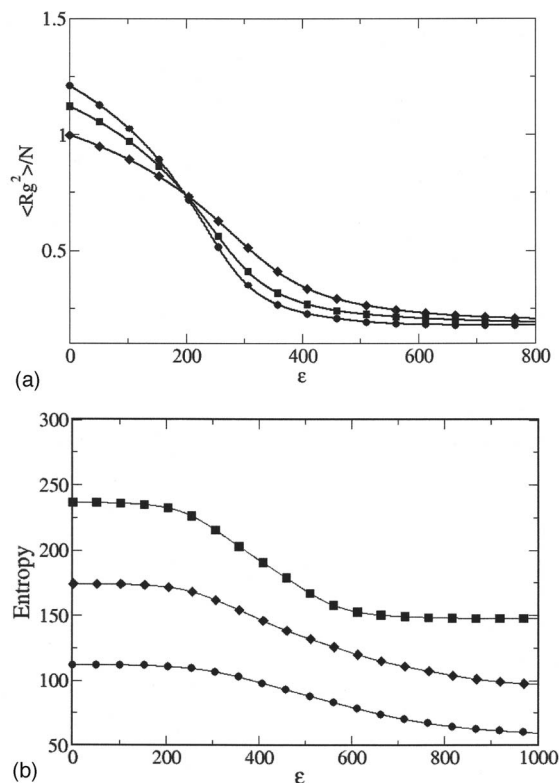


FIG. 4. (a) Plot of the mean square radius of gyration, $\langle R_g^2 \rangle / N$, as a function of epsilon, ϵ , in the high-temperature regime, $T=500$ K. The parameters are (♦) $N=30$ beads, (■) $N=45$ beads, and (●) $N=60$ beads. (b) Plot of chain entropy as a function of epsilon, ϵ , for various chain lengths in the high-temperature regime, $T=500$ K. The parameters are (●) $N=30$ beads, (♦) $N=45$ beads, and (■) $N=60$ beads.

tractive interactions increasing proportionally to $(DP)^2$ (degree of polymerization) while the chain entropy increases only linearly with DP. Thus, the longer the chain, the lower the value of ϵ needed for the transition to occur.

Figure 4(b) shows the configurational entropy of the chain as a function of ϵ for various chain lengths. It is clear from the figure that the entropy decreases with increasing ϵ , as expected. Moreover, for large values of ϵ , the entropy levels off. Similar to the previous figure, the transition becomes sharper with increasing chain length. This increase in the sharpness of the transition implies its increasing cooperative nature. This cooperative nature of the coil-globule transition has also been discussed by Kuznetsov and Grosberg.⁴³ Figure 4(b) also shows that the transition shifts towards lower values of ϵ with an increase in chain length. Again, such a shift can be explained by the scaling arguments presented in the previous paragraph. It is interesting to note that the transition seems to occur at different values of ϵ when Figs. 4(a) and 4(b) are compared. Further analysis shows that the decrease in the entropy of the chain with increasing ϵ is negligible until the value of ϵ is large enough to completely overwhelm the effect of excluded volume interactions. This implies that the entropy of the chain remains approximately constant until the chain has collapsed, $\epsilon \sim 400$ in Fig. 4(a). Only when the chain is almost collapsed the entropy of the chain decreases with increasing ϵ .

Finally, we note that helical properties such as the helical

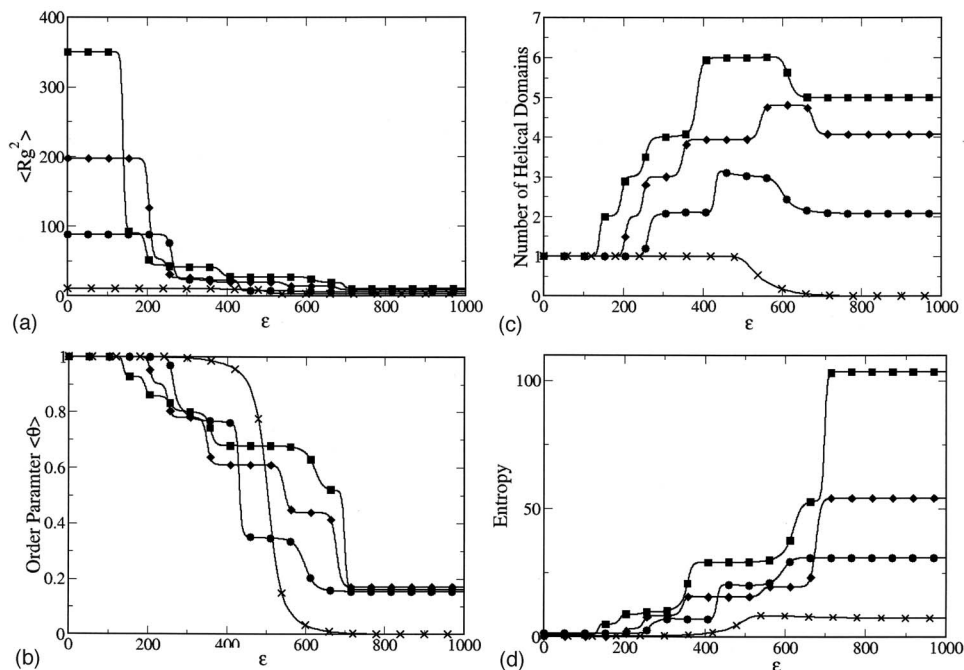


FIG. 5. (a) Plot of the mean square radius of gyration, $\langle R_g^2 \rangle$, as a function of epsilon, ϵ , for various chain lengths in the low-temperature regime. The parameters are (*) $N=10$ beads, (●) $N=30$ beads, (◆) $N=45$ beads, and (■) $N=60$ beads. (b) Plot of the order parameter, $\langle \theta \rangle$, as a function of epsilon, ϵ , for various chain lengths in the low-temperature regime. The parameters are (*) $N=10$ beads, (●) $N=30$ beads, (◆) $N=45$ beads, and (■) $N=60$ beads. (c) Plot of the number of helical domains, $\langle N_H \rangle$, as a function of epsilon, ϵ , for various chain lengths in the low-temperature regime. The parameters are (*) $N=10$ beads, (●) $N=30$ beads, (◆) $N=45$ beads, and (■) $N=60$ beads. (d) Plot of chain entropy as a function of epsilon, ϵ , for various chain lengths in the low-temperature regime. The parameters are (*) $N=10$ beads, (●) $N=30$ beads, (◆) $N=45$ beads, and (■) $N=60$ beads.

content and number of helical domains do not provide any additional insight into the coil-globule transition as these properties are all very close to zero in the high-temperature regime.

3. The low T regime

As discussed previously, in the low-temperature regime, we observe a cascade of *continuous conformational* transitions which involve the collapse of the helical structure with increasing ϵ . The sharpness of these transitions is a direct result of the competition between various stable states that are present at low temperatures. In this section, we analyze these transitions using various configurational, conformational, and thermodynamic properties along with their chain length dependences.

We start with the analysis of the mean square radius of gyration, $\langle R_g^2 \rangle$, as a function of ϵ [Fig. 5(a)] for chains with 10, 30, 45, and 60 beads. As expected, the figure shows a decrease in $\langle R_g^2 \rangle$ with increasing ϵ indicating a collapse of the chain into more compact configurations. While for $DP=10$ only one, sharp decrease is observed, the case is different for $DP=30, 45$, and 60 . For these chain lengths a series of sharp, but continuous decreases in $\langle R_g^2 \rangle$ is observed at specific values of ϵ . These changes in $\langle R_g^2 \rangle$ clearly indicate a substantial change in the dimensions of the chain which implies the collapse of the helical structure upon an increase in ϵ . Moreover, these changes indicate that the molecular mechanism behind the collapse of the chain is related to the breaking of the helical structure.

It is also interesting to observe that in some windows of

ϵ , long chains have *smaller* dimensions than short ones. This happens because long chains undergo the first transition before the short ones. This behavior is a clear illustration of the effect of chain length and how it modifies the state diagram and physical properties of the chain. A more detailed discussion is given below.

To validate this argument, we plot the order parameter, $\langle \theta \rangle$, in Fig. 5(b) as a function of ϵ . It is clear from the figure that for small values of ϵ , the chain is in the helical state. However, as ϵ increases, $\langle \theta \rangle$ decreases in a steplike manner at the same values of ϵ as in the case of $\langle R_g^2 \rangle$; hence, supporting our argument about the mechanism responsible for the collapse of the chain. As expected, we observe only a single transition for $DP=10$ and a cascade of steplike transitions for $DP=30, 45$, and 60 . Moreover, for the latter, we observe residual secondary structure in the collapsed globular configuration of the chain which mimics the collapse states of many proteins.⁴²

The decrease of the order parameter is due to the breaking of the helical structure caused by the interbead, long-range attractive interactions and was observed for all chain lengths studied (10, 30, 45, and 60 beads). This mechanism is similar to the one present in the standard helix-coil transition of long enough chains where the polymer undergoes the transition by breaking the all-helical conformation into shorter helical strands as the temperature is increased. However, the helix-coil transition does not consider long-range interactions and the helical strands do not aggregate like in this case. Since the underlying mechanisms for breaking the helical structure are similar, cooperativity is expected to occur in the various, low-temperature transitions. This observa-

tion agrees with the experiments of Moore and co-workers⁴⁴ who studied the helix-coil transition of phenylene-ethynylene oligomers at constant temperature as a function of solvent quality and observed the typical sigmoid-type shape of $\langle\theta\rangle$ which indicates cooperativity. However, they observed only one transition which is due to the low DP used in their studies. Interestingly, as mentioned before, we also observe only a single transition when we studied chains with 10 beads.

Figure 5(c) provides further insight into the behavior of the system at low temperatures; we plot the number of helical strands, $\langle N_H \rangle$, as a function of ε for various chain lengths. Apart from the case of chain length equal to 10, the figure shows that for all other chain lengths, $\langle N_H \rangle$ first increases and then decreases before reaching a constant value for large values of ε . In order to understand this interesting, nonmonotonic behavior we notice that, although $\langle N_H \rangle$ increases due to the breaking of helical structure, the total helical content, i.e., order parameter, decreases monotonically. This leads to the conclusion that there should be a maximum in the dependence of $\langle N_H \rangle$ on ε after which $\langle N_H \rangle$ should begin to decrease with increasing ε . Moreover, the maximum in $\langle N_H \rangle$ depends on the length of the chain. In our case, this happens when $\langle N_H \rangle$ is equal to 3, 5, and 6 for chain lengths of 30, 45, and 60 beads, respectively. However, $\langle N_H \rangle$ does not approach zero on further increase of ε which implies that some residual secondary structure remains even for large values of ε where the chain becomes a collapsed globule. This residual structure can be melted with an increase in temperature. This behavior can also be observed in Figs. 2(b)–2(d) (high ε regime) for chain lengths equal to 30, 45, and 60 beads, respectively.

Let us now discuss the fundamental differences in the behavior of $\langle N_H \rangle$ in the low T and low ε regimes for long chains. Previously, it was said that in the low ε regime $\langle N_H \rangle$ first increases with increasing temperature in continuous fashion before decaying down to zero. During this transition no specific configurations of the chain could be identified. This was due to the fact that when the temperature is increased and the helix breaks into shorter helical strands, it does so in such a way that the shorter helical strands can have any orientation in space and, moreover, can have any length within the limitation imposed by the total length of the chain. This generates a very large number of possible configurations with similar values of $\langle N_H \rangle$. In this case, there is no reason for the helix to break into shorter helices of specific length and with a specific orientation. This is a consequence of the small value of ε where long-range interactions are weak. What is observed is an ensemble average of the number of helical domains as a function of temperature. However, in the low T limit, the situation is different. As ε increases, the long-range interactions become stronger and start to control the behavior of the chain. When they are strong enough to break the helix, these long-range attractions are the ones that determine the set of configurations of the chain that are the most stable ones. These configurations are the ones where there are two helical strands parallel to each

other and in spatial contact. Thus, the difference in the molecular mechanisms active in both regimes is due to the presence of the long-range interactions.

Figures 5(a)–5(c) clearly show that an increase in the length of the chain enriches the physics of the state diagram with novel, stable conformations of the chain. Indeed, a number of new conformations with more helical strands appear between the all-helical and the collapsed globular conformations. Therefore, more and sharper transitions are observed in the low-temperature regime. However, due to finite size effects, they are not transitions in the *thermodynamic* sense as discussed by Stukan *et al.*⁴⁵ Moreover, the dependence on chain length follows the opposite trend reported for semiflexible chains. The decrease in $\langle R_g^2 \rangle$ and $\langle\theta\rangle$ together with the changes in $\langle N_H \rangle$ described in Figs. 5(a)–5(c) support the proposed mechanism for the breaking of the helical structure which is illustrated in Figs. 2(b)–2(d) with several snapshots of the polymer chain.

During the first steplike transition, the all-helical conformation breaks into two shorter, but relatively long, helical strands which may have any relative orientation in space. However, the most probable configuration is the one where they are aligned parallel to each other and are located side by side, as shown in Figs. 2(b)–2(d). This relative alignment is favored by the increase in the number of contacts between the beads of both helical strands which decreases the LJ interaction energy and the helical conformation of both strands which decreases the torsional energy. This first transition was observed for all chain lengths studied (30, 45, and 60) making it a characteristic feature of the model. Furthermore, we would like to emphasize here that the first transition shifts to lower values of ε as the chain length increases, as depicted in Fig. 5(b). This shift results from a similar argument to the one discussed previously for the coil-globule transition, but with a small modification. On one hand, the LJ attractive interaction among beads increases as $(DP)^2$ while, on the other hand, the helical interactions increase linearly with DP. Hence, the LJ interactions overwhelm the enthalpy gain due to the formation of longer or more helices as the chain length increases. Thus, smaller values of ε are required to break various structures. For example, for 30-, 45-, and 60-bead chains at 200 K the all-helical conformation breaks around $\varepsilon \approx 300$, 225, and 175, respectively.

A further increase in ε leads to a transition to a configuration with three helical strands parallel to each other. Interestingly, this transition was also observed for all the chain lengths studied. Further increases in ε take the system into new regimes with more helical strands parallel to each other. Also, the same energetic argument used to rationalize the formation of the first state is also applicable to the other states until the LJ attractive interactions overwhelm the formation of helices and control the behavior of the chain.

The length of the chain has a fundamental effect on the number and characteristics of each of these new, low-temperature states. An increase in the length of the chain increases the number of the low-temperature, intermediate states. For example, in the case of 60 beads in Fig. 2(d), we observe configurational states with four and six helical strands parallel to each other. However, the parallel align-

ment of the helices is disturbed by the large number of coil beads at higher values of ε . Here, we detect a transition between two configurational states, both with six helical strands, where the main difference is the degree of alignment of the strands resulting from higher value of ε and less helical beads. A similar behavior was also observed for chains with 45 beads in Fig. 2(c). In some cases, we also observe that $\langle N_H \rangle$ does not have an integral value. This kind of behavior suggests that, in such cases, there exist two or more stable states with similar free energies, each having the same order parameter but different numbers of helical strands, and all of them contribute to the partition function significantly. One of such cases was observed in Fig. 2(c) for 45 beads in $\varepsilon \sim 300$ and $T \sim 170\text{--}250$ range, where we observe $\langle N_H \rangle \sim 4.3$. In all cases, we observe a final, stable collapsed globular configuration with residual secondary structure where the number of helices (local residual secondary structure) increases with chain length, i.e., 2, 4, and 5 for chain lengths of 30, 45, and 60 beads, respectively. In addition, the degree of alignment seems to change with changes in chain length. For example, for the 30-bead case the residual helical strands were found to be parallel to each other unlike the 60-bead case where the five residual strands were observed to be in a nonparallel configuration.

The picture that has emerged from our study is also supported by thermodynamic properties such as entropy which is plotted in Fig. 5(d) for chain lengths equal to 10, 30, 45, and 60 in the low-temperature regime. For small values of ε , we observe that the entropy is close to zero for all the chain lengths studied. This is a consequence of the all-helical configuration of the chain. However, as the various transitions start to occur, we observe a sharp increase in entropy with increasing ε . Note that all the transitions in the entropy occur at the same values of ε where the other configurational and conformational properties showed sharp changes. The increase in entropy with each transition suggests that there are many conformations of the chain in each low-temperature regime, similar to the case of the collapsed globule at high temperatures. This provides further proof that the low-temperature regimes cannot be associated with specific structures of the chain but rather with ensembles of various conformations of the chain *that are geometrically similar*.

Let us look at the last statement from a different and refreshing perspective: the one of protein folding funnels.⁴⁶ Helical macromolecules can be considered to be the simplest possible model proteins. Therefore, the Levinthal paradox⁴⁷ and its solution via the concept of protein folding funnels should also manifest themselves in models of helical macromolecules. So, we ask the following: Is this the case of our model? The answer is yes. Our model for the macromolecule has a countable number of configurations equal to 64^{N-3} where N is the number of beads. Thus, for a chain with 10 (60) beads the total number of possible configurations is $\sim 10^{12}$ ($\sim 10^{103}$). Even for the shortest chain the generation of 10^{12} configurations is a computationally very intensive or even an impossible task; the generation of 10^{103} configurations is out of the question. Thus, our model has the same limitations as real proteins: an extremely large number of configurations which forbids an exhaustive random sampling

of the configurational space. This is at the basis of the Levinthal paradox. Our model also realizes the concept of protein folding funnels which are defined as “a collection of geometrically similar collapsed structures, one of which is thermodynamically stable with respect to the rest, though not necessarily with respect to the whole conformation space.”⁴⁶ This is precisely what the last sentence in the previous paragraph suggests. Therefore, each of the low-temperature regimes corresponds to one folding funnel and our simulation study is capable of identifying the geometrical characteristics of each of them.

IV. CONCLUSIONS

In the present article, we have shown that the overall three-dimensional structure of a helical polymer is the consequence of a delicate balance between short-range, secondary and long-range, tertiary interactions. In our simulations, this interplay has been shown to occur at low temperatures where both interactions are significant. The strength of tertiary interactions has been shown to have a significant effect on the folding or collapse of the helical macromolecule. Moreover, this effect increases with increasing chain length as seen by the increase in the number of low-temperature transitions with increasing chain length.

The importance of long-range interactions in the determination of the overall three-dimensional conformational state of the chain, in addition to secondary interactions, points to the relevant role played by the surrounding environment on the folding of helical and more complex macromolecules such as proteins. This indicates that a more detailed modeling of the surrounding solvent is required to refine our current model. We will pursue this study in a future publication.

For weak tertiary interactions and at high temperatures, our model predicts the occurrence of the helix-coil and coil-globule transitions, respectively. However, under these circumstances, these transitions are independent of each other. However, as the temperature is reduced and ε is increased, these transitions get coupled and interfere with each other. The result of this coupling is the emergence of a plethora of novel conformational states which are stable at low temperatures. These states were found to be ensemble averages of conformations with similar characteristics; for example, all the conformations in one state had the same number of helical strands. Moreover, they are separated by transition lines where the polymer undergoes a substantial change in its configurational, conformational, and thermodynamic properties.

The analysis of many properties led to the conclusion that as ε increases and the polymer crosses the transition lines, the helical strands break into shorter ones which adopt a parallel configuration to minimize the Lennard-Jones interactions. With further increase in ε , as helical strands get shorter, the parallel orientation of such strands also gets perturbed until the globular state with residual secondary structure is reached. Further increase of the strength of the tertiary interactions did not lead to any new structure of the chain.

Finally, the effect of geometrical parameters such as bond lengths, bond angles, and others has not been fully

explored. Changes in the values of these parameters would definitely affect the distribution of the various possible states in the state diagram, especially in the low T regime. However, we expect that the overall features of the transitions along with the rich phase behavior of state diagrams would still persist independently of the choice of the values of the parameters used.

ACKNOWLEDGMENTS

This material is based upon work partially supported by the National Science Foundation under Grant No. CHE-0132278. Also, acknowledgment is made to the Donors of The Petroleum Research Fund, administered by the American Chemical Society, for partial support of this research (PRF No. 37051-G7) and The Ohio Board of Regents, Action Fund (Grant No. R566).

- ¹A. Y. Grossberg and A. R. Khovolov, *Statistical Physics of Macromolecules* (AIP, New York, 1994); W. H. Stockmayer, *Makromol. Chem.* **35**, 54 (1960).
- ²Z. Cao, W. Liu, P. Gao, K. Yao, H. Li, and G. Wang, *Polymer* **46**, 5268 (2005).
- ³R. Kita and S. Wiegand, *Macromolecules* **38**, 4554 (2005).
- ⁴M. O. Gallyamov, A. R. Khokhlov, and M. Moller, *Macromol. Rapid Commun.* **26**, 456 (2005).
- ⁵R. S. Dias, J. Innerlohinger, O. Glatter, M. G. Miguel, and B. J. Lindman, *J. Phys. Chem. B* **109**, 10458 (2005).
- ⁶S. M. Mel'nikov, V. G. Sergeev, and K. Yoshikawa, *J. Am. Chem. Soc.* **117**, 2401 (1995).
- ⁷C. Wu and X. Wang, *Phys. Rev. Lett.* **80**, 4092 (1998).
- ⁸X. Qui, M. Li, C. M. S. Kwan, and C. Wu, *J. Polym. Sci., Part B: Polym. Phys.* **36**, 1501 (1998).
- ⁹P. J. Flory, *Principles of Physical Chemistry* (Cornell University Press, Ithaca, NY, 1953).
- ¹⁰S. Doniach, T. Garel, and H. Orland, *J. Chem. Phys.* **105**, 1601 (1996).
- ¹¹Z. Luthey-Schulten, B. E. Ramirez, and P. G. Wolyens, *J. Phys. Chem.* **99**, 2177 (1995).
- ¹²S. Tadaka, Z. Luthey-Schulten, and P. G. Wolyens, *J. Chem. Phys.* **110**, 11616 (1999).
- ¹³D. M. Duffy and P. M. Rodger, *J. Am. Chem. Soc.* **124**, 5206 (2002).
- ¹⁴V. A. Ivanov, M. R. Stukan, V. V. Vesilevskaya, W. Paul, and K. Binder, *Macromol. Theory Simul.* **9**, 488 (2000).
- ¹⁵J. A. Martemyanova, M. R. Stukan, V. A. Ivanov, M. Muller, W. Paul, and K. Binder, *J. Chem. Phys.* **122**, 174907 (2005).
- ¹⁶F. Rampf, W. Paul, and K. Binder, *Europhys. Lett.* **70**, 628 (2005).
- ¹⁷J. G. Saven and P. G. Wolynes, *J. Mol. Biol.* **257**, 199 (1996).
- ¹⁸J. J. Chou and E. I. Shakhnovich, *J. Phys. Chem. B* **103**, 2535 (1999).
- ¹⁹E. A. Di Marzio, *Prog. Polym. Sci.* **24**, 329 (1999); *J. Chem. Phys.* **119**, 6378 (2003).
- ²⁰A. J. Matsuyama, *Chem. Phys.* **121**, 604 (2004).
- ²¹D. Poland and H. A. Scheraga, *Theory of Helix-Coil Transition in Biopolymers* (Academic, New York, 1970).
- ²²M. Karplus and E. I. Shakhnovich, in *Protein Folding*, edited by T. Creighton (Freeman, New York, 1992).
- ²³U. H. E. Hansmann and Y. Okamoto, *J. Comput. Chem.* **14**, 1333 (1993); Y. Okamoto and U. H. E. Hansmann, *J. Phys. Chem.* **99**, 11276 (1995).
- ²⁴F. Wang and D. P. Landau, *Phys. Rev. Lett.* **86**, 2050 (2001).
- ²⁵N. Rathore and J. J. de Pablo, *J. Chem. Phys.* **116**, 7225 (2002).
- ²⁶N. Rathore, T. A. Knotts, and J. J. de Pablo, *J. Chem. Phys.* **118**, 4285 (2003).
- ²⁷N. A. Volkov, A. A. Yurchenko, A. P. Lyubartsev, and P. N. Vorontsov-Velyaminov, *Macromol. Theory Simul.* **14**, 491 (2005); *J. Phys. A* **37**, 1573 (2004).
- ²⁸Y. Sliozberg and C. F. Abrams, *Macromolecules* **38**, 5321 (2005).
- ²⁹G. L. Thomas, R. B. Sessions, and M. J. Parker, *Bioinformatics* **21**, 2839 (2005).
- ³⁰P. Pliego-Pastrana and M. D. Carbajal-Tinoco, *J. Chem. Phys.* **122**, 244908 (2005).
- ³¹A. Cavalli, M. Vendruscolo, and E. Paci, *Biophys. J.* **88**, 3158 (2005).
- ³²V. Varshney, T. E. Dirama, T. Z. Sen, and G. A. Carri, *Macromolecules* **37**, 8794 (2004).
- ³³V. Varshney and G. A. Carri, *Phys. Rev. Lett.* **95**, 168304 (2005).
- ³⁴E. Eisenriegler, *Polymers Near Surfaces* (World Scientific, Singapore, 1993).
- ³⁵G. A. Carri and M. Muthukumar, *Phys. Rev. Lett.* **82**, 5405 (1999).
- ³⁶W. L. Mattice and U. W. Suter, *Conformational Theory of Large Molecules* (Wiley, New York, 1994).
- ³⁷B. M. Budak and S. V. Fomin, *Multiple Integrals, Field Theory and Series* (MIR, Moscow, 1973).
- ³⁸G. A. Carri (unpublished).
- ³⁹Q. Yan, R. Faller, and J. J. de Pablo, *J. Chem. Phys.* **116**, 8745 (2002).
- ⁴⁰V. Varshney and G. A. Carri, *Macromolecules* **38**, 780 (2005).
- ⁴¹B. J. Schulz, K. Binder, M. Müller, and D. P. Landau, *Phys. Rev. E* **67**, 067102 (2003).
- ⁴²P. Romiszowski, *Biopolymers* **54**, 262 (2000).
- ⁴³D. V. Kuznetsov and A. Y. Grosberg, *Macromolecules* **25**, 1970 (1992).
- ⁴⁴R. B. Prince, J. G. Saven, P. G. Wolynes, and J. S. Moore, *J. Am. Chem. Soc.* **121**, 3114 (1999); J. C. Nelson, J. G. Saven, J. S. Moore, and P. G. Wolynes, *Science* **277**, 1793 (1997).
- ⁴⁵M. R. Stukan, V. A. Ivanov, A. Y. Grosberg, W. Paul, and K. Binder, *Chem. Phys.* **118**, 3392 (2003) and references therein.
- ⁴⁶P. E. Leopold, M. Montal, and J. N. Onuchic, *Proc. Natl. Acad. Sci. U.S.A.* **89**, 8721 (1992).
- ⁴⁷C. Levinthal, *J. Chim. Phys. Phys.-Chim. Biol.* **65**, 44 (1968); in *Mossbauer Spectroscopy in Biological Systems*, edited by P. Debrunner, J. C. M. Tsibris, and E. Munck (University of Illinois Press, Urbana, 1969), pp. 22–24; R. Zwanzig, A. Szabo, and B. Bigchi, *Proc. Natl. Acad. Sci. U.S.A.* **89**, 20 (1992); E. A. Di Marzio, *Prog. Polym. Sci.* **24**, 329 (1999).